# Electronic energy-loss mechanisms for H, He, and Ne in TiN

M. A. Sortica,[1,*] V. Paneta,[1] B. Bruckner,[1,2] S. Lohmann,[1] M. Hans,[3] T. Nyberg,[4] P. Bauer,[2] and D. Primetzhofer[1]

[1]*Department of Physics and Astronomy, Uppsala Universitet, Box 516, S-751 20 Uppsala, Sweden*

[2]*Atomic Physics and Surface Science, Johannes Kepler University, A-4040 Linz, Austria*

[3]*Materials Chemistry, RWTH Aachen University, D-52074 Aachen, Germany*

[4]*Department of Engineering Sciences, Uppsala Universitet, Box 534, S-751 20 Uppsala, Sweden*

(Received 9 June 2017; published 6 September 2017)

The specific energy loss of medium-energy hydrogen, helium, and neon ions in titanium nitride is studied. Electronic stopping cross sections of ions in the energy range of 3–140 keV/amu were measured in backscattering geometry using time-of-flight medium-energy ion scattering, from the energy loss experienced in TiN thin films on Si. For the lowest energies, data for H show a strong deviation from Bragg's rule. For hydrogen and Ne ions, electronic stopping exhibits velocity proportionality at ion velocities below 1 a.u. Comparison to density functional theory calculations of the stopping power yields very good agreement for H, while for He and Ne, the experimentally observed electronic stopping power is considerably higher than predicted. For He the extrapolation of the stopping power at low energies points to a nonvanishing energy loss at vanishing ion velocity. The present data can thus be taken as an indication of additional energy-loss processes different from direct electron-hole pair excitation. Furthermore, the results provide reference values for ion-beam-based analysis of TiN, a material with huge technological relevance.

DOI: 10.1103/PhysRevA.96.032703

## I. INTRODUCTION

The interaction of energetic ions with matter leads to a deceleration of the intruding particles due to interaction with both target nuclei and electrons, processes referred to as nuclear and electronic stopping, respectively. Precise knowledge on the specific amount of energy deposited is of relevance for understanding the processes and applications in such different areas as nanotechnology (ion-beam patterning, ion implantation) [1,2], fusion research (plasma-wall interaction) [3], or medicine (hadron therapy) [4]. Apart from that, it is a key quantity for establishing depth profiles in most ion-beam-based analytical tools [5,6] and an interesting fundamental playground for testing the accuracy of calculations and theoretical considerations in the field of many-particle physics [7–9].

The experimentally accessible key quantity with highest relevance for the above-mentioned applications is the mean energy loss per path length, $dE/dx$, which has the dimension of a force and is typically referred to as the stopping power, $S$, of the material for a certain ion species [10]. Alternatively, and in order to avoid a dependence on the potentially unknown target density, the more convenient stopping cross section (SCS) $\varepsilon$, defined via $\varepsilon = (1/n)dE/dx$ with $n$ the atomic number density, can be employed. At high energies, on the order of several hundred keV/amu, the energy loss is almost exclusively due to excitation of the only weakly perturbed electronic system of the target material in binary interactions. With decreasing particle energies, several factors add complexity to both the theoretical description as well as the experimental possibilities to extract the stopping power and disentangle its components. At first, all scattering cross sections for charged particles show a strong dependence on the ion energy [11]. Single-scattering models may have to be abandoned and only Monte Carlo calculations permit accurately describing the energy loss due to elastic scattering for a specific experimental geometry.

Additionally, the decreasing maximum energy transfer in binary encounters between the projectile and electrons induces increasing effects from limited availability of unoccupied states when interacting with bound electrons. Eventually, the different impact parameters probed at lower energies [12] and the decreasing charge state of the penetrating particle [13] lead to a maximum ("Bragg peak") of the observed electronic stopping power, which is observed, e.g., at around 100 keV for protons.

At lower energies the interaction is to a large extent limited to valence and conduction electrons, which effectively screen the projectile charge, and make the stopping power prone to chemical matrix effects [14,15], different from the well-established Bragg's rule valid at sufficiently high energies [16]. A simple but powerful way to model the involved electronic states is in terms of a free-electron gas (FEG), which provides an accurate description of the ion-electron Coulomb interactions especially at sufficiently high ion velocities [17]. This approach has been continuously refined [18,19] and for low ion velocities, i.e., energies significantly below the stopping maximum, it results in velocity-proportional electronic stopping power $S = Q(Z_1, r_s)v$. $Q$ is commonly referred to as the friction coefficient of the FEG, which depends on the atomic number of the ion $Z_1$, and the FEG density parameter $r_s$, i.e., the Wigner-Seitz radius of the sphere containing one electron, usually given in a.u. [20].

With the advent of modern computer calculations, density functional theory (DFT) permitted predicting electronic stopping power for a FEG of different densities [21,22]. In a nonlinear calculation based on DFT calculations of the induced electron density, Echenique *et al.* evaluated the friction coefficients for ions in the range $1 \leqslant Z_1 \leqslant 18$ [23]. For heavier ions, this model yields $Z_1$ oscillations in the electronic stopping power, as observed experimentally for slow ions

*mauricio.sortica@physics.uu.se

 

channeled in Si [24]. For this ion target combination and the density of valence electrons characterized by $r_s = 2.28$ [25], the experimentally observed oscillations of the stopping power with $Z_1$ could be modeled with a minimum at $Z_1 = 10$ or 11 and a maximum for $Z_1 = 6$ or 7, depending on the FEG density.

Indeed, in particular for protons, in most materials velocity-proportional energy loss is observed at low ion velocities [26]. For protons, it has been found appropriate to characterize the valence electron density by the experimentally observed plasmon frequency, $\hbar\omega_{\mathrm{p,expt}}$ [27]. Several systems, however, in particular noble metals, have shown a changing slope in the velocity scaling of the electronic stopping cross sections for low ion velocities [28]. The nonlinear velocity scaling was found persistently for polycrystalline and single-crystalline materials as well as in different experimental approaches, i.e., backscattering and transmission [29,30]. This fact was interpreted by the contributions of different electronic states with finite excitation thresholds such as the *d* bands in Au or Cu. This interpretation has also been corroborated by time-dependent DFT (TD-DFT) calculations [31], which showed the nonlocal character of involved electronic transitions at low energies [32]. For insulators, all electronic states show excitation thresholds, which has in fact been confirmed experimentally by different approaches [33–35]. The threshold energies, however, below which electronic stopping was found to vanish, are different compared with expectations for an unperturbed electronic system [36]. Here also, huge efforts have led to an improved theoretical description of the processes observed, which actually includes charge transfer different from collisions directly exciting electron-hole pairs [37,38].

For ions heavier than protons, the situation is expected to be more complex, due to the fact that the ions will be dressed to a different extent by electrons [39]. Indeed, experiments have shown that the energy loss of helium and proton ions can often not be explained on common ground: The energy loss of He in $SiO_2$ was found to show a different threshold behavior [30]. Within the FEG model, substantially different electron densities have to be employed to explain the observed magnitude of the electronic energy loss for He [40,41]. Additionally, nonlinearities in the energy loss have been demonstrated experimentally, which cannot be described in binary encounter models [42]. One possible explanation as well as illustration of the complexity of the projectiles is the ability of additional large energy transfers due to internal excitation of the projectile and subsequent excitation of the target electronic system [43,44].

In the present study we investigate electronic stopping in titanium nitride for energies around and below the stopping maximum. For this purpose we have studied energy loss of H, D, He, and Ne ions in TiN thin films by time-of-flight medium-energy ion scattering (TOF-MEIS) and Monte Carlo simulations. Ultrathin-film targets with thicknesses of at most several tens of nanometers grown by sputtering and arc deposition were employed to exclude a substrate bias. The results show a strong qualitative difference in the observed velocity dependence of electronic stopping for protons, helium, and neon ions which for projectiles heavier then protons indicates a substantial contribution of processes dissipating energy in a way different from direct excitation of electron-hole pairs.

## II. EXPERIMENTS

Thin films were grown on Si substrates by different means. Both sputtering and arc deposition were employed. Additionally, films with a W $\delta$ layer of about 1 nm thickness at the interface between the substrate and the TiN thin film were grown for backscattering experiments employing heavier ion species.

Sputter depositions were carried out in a cylindrical UHV chamber (Kurt J. Lesker CMS-18) equipped with a load lock and evacuated through a cryopump (CTI Cryo-Torr 8). The base pressure was below $10^{-5}$ Pa. The substrate table was rotated at 20 rpm and kept at floating potential. The pulsed dc power to the target was supplied by an Advanced Energy Pinnacle Plus power supply. The 3-in. Si wafers were dipped into hydrofluoric acid solution prior to deposition. Only nitrogen [30 SCCM (cubic centimeter per minute at STP)] was introduced in the chamber and the processing pressure was kept at 0.12 Pa. The substrate temperature was kept at 750 °C and the 4-in. target was fed with 800 W of pulsed dc (resulting in a target current of 1.35 A) with a frequency of 50 kHz and a pulse off-time of 0.5 $\mu$s.

For the W $\delta$-layer deposition, a 4–in. target was used and 60 SCCM of Ar was introduced and the pressure was kept at 0.40 Pa. The pulsed dc power was 200 W (0.42 A) with a pulse frequency of 250 kHz and a pulse off-time of 0.5 $\mu$s.

Polycrystalline TiN thin films with NaCl-like B1 cubic structure were also synthesized by cathodic arc evaporation in an Oerlikon Balzers INGENIA P3e industrial batch coating system. Si (100) 2-in. wafers were assembled on the twofold rotation carousel and the base pressure was below $2\times10^{-4}$ Pa. Thin films were synthesized at 420 °C in an $Ar/N_2$ atmosphere with 100 SCCM Ar flow and 3.5 Pa deposition pressure, while the substrate bias potential was −100 V. The venting temperature after deposition was below 65 °C to minimize surface-near oxygen uptake [45]. Targeted film thicknesses of 200 and 20 nm were obtained by adjusting the deposition time and evaluated by scanning electron microscopy on fracture cross sections.

Characterization of the obtained thin films was performed by Rutherford backscattering spectrometry (RBS) employing 2 MeV $^4He^+$ ions provided by a 5 MV 15SDH-2 tandem accelerator to obtain a reliable thickness calibration. The film thicknesses obtained were 16.5 nm (sputter deposited) and 18.9 nm (arc deposited), as well as 17.5 nm (for the sputtered film with a $\delta$ layer). Note that these are nominal thicknesses assuming bulk density. Time-of-flight elastic recoil detection analysis (TOF-ERDA) characterization of the samples with a $^{127}I^{8+}$ primary beam was employed to guarantee accurate stoichiometry and to check for impurities of the employed thin films. Measurements confirmed the expected film stoichiometry of $Ti/N = 1 \pm 0.08$ and showed only minor surface impurities of oxygen. Details on the employed TOF-ERDA setup can be found in Zhang *et al.* [46]; details of the evaluation are discussed in the supplements of Arvizu *et al.* [47].

To extract energy-loss data, ion scattering experiments were performed in backscattering geometries employing the TOF-MEIS setup at Uppsala University [48]. For H, both protons and molecular ions were used in an equivalent proton energy range from 8.5 to 140 keV. For He, ion energies ranged from 25

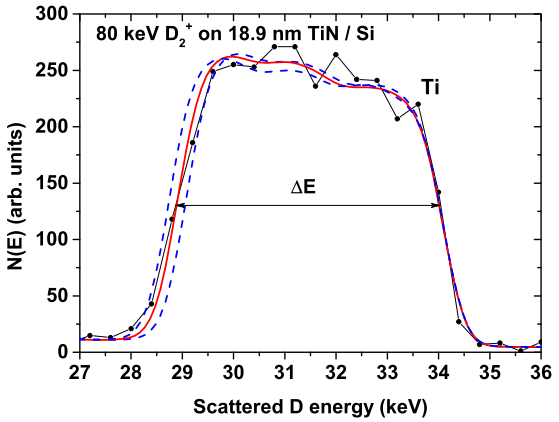


FIG. 1. Energy-converted TOF-MEIS spectrum for 80 keV $D_2^+$ scattered from a titanium nitride film (black dots). The corrected stopping power is obtained from fitting of the Ti peak width ($\Delta E$) by TRIM for backscattering (TRBS) simulation (solid red line). Dashed blue lines are simulations for $\pm 4\%$ deviation on the electronic stopping power.

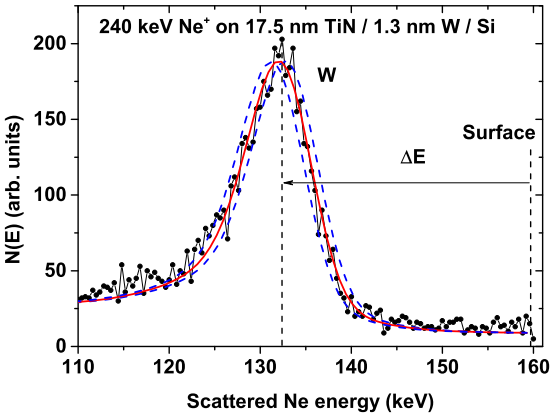


FIG. 2. Energy-converted TOF-MEIS spectrum for 240 keV $Ne^+$ scattered from a sample consisting of a titanium nitride film on silicon with a $\delta$ layer of tungsten (black dots). Through TRBS simulation, the corrected stopping power is obtained from the shift of the W peak position ($\Delta E$) due to ion interaction with TiN film (solid red line). Dashed blue lines are simulations for $\pm 4\%$ deviation on the electronic stopping power.

to 220 keV and for Ne from 60 to 320 keV. The energy ranges were chosen such that within the capabilities of the machine a similar velocity regime was probed. A large position-sensitive detector ($\Omega > 0.1$ sr) was employed for detecting backscattered particles irrespective of their charge state. The large area of the detector permits acquiring spectra for doses of at most several tens of nC, which permits measurements without any significant damage to the samples even for heavier projectiles such as Ne. However, only about 20% of the active detector surface was employed for spectrum acquisition to avoid geometrical straggling due to different scattering angles contributing to the data. Energy conversion of obtained TOF data can be performed from the well-known sample-detector distance and the prompt photon signal observed from the sample for the impinging ion packages [49]. An example of an energy-converted TOF-MEIS spectrum for 80 keV $D_2^+$ scattered from TiN on Si is shown in Fig. 1.

For H and He, data were mainly obtained from evaluating the width of the obtained spectral features due to scattering from Ti. This width is a direct measure of the film thickness as well as specific energy loss in the material. Note that experiments were performed on thin films grown by cathodic arc as well as sputter deposition, to check for potential influences of the films' microstructure on the data obtained. For Ne, due to unfavorable scattering kinematics, the ions scattered from a W$\delta$ layer were used as a marker for the energy loss experienced in the thin film by comparing the peak position with the expected energy in absence of a TiN thin film (see Fig. 2). For He ions control measurements were performed for both approaches yielding equivalent results within the experimental uncertainty.

To properly disentangle electronic stopping from nuclear energy losses and address also the issue of path length straggling, evaluation was performed by simulating experimental spectra with the help of Monte Carlo simulations by the TRIM for backscattering code (TRBS) [50]. The program package permits employing different interatomic potentials with adjustable screening length corrections. For the present energies, an uncorrected Ziegler-Biersack-Littmark (ZBL) potential was found to sufficiently well describe the multiple scattering background observed in particular for low energies. The correct electronic stopping power can be obtained by simulating the experiment and subsequently tuning the employed stopping power in the simulation until a good fit with the experimental data is obtained. In this procedure, a correction factor to the electronic stopping power modeled as in SRIM [51] is employed. This also implies that the velocity dependence of the model is not changed, which, however, is expected to have only minor influence on results as long as the total observed energy losses are small relative to the employed energies, i.e., $\Delta E/E \ll 1$. Additionally, it is possible to employ a different scaling behavior in TRBS, if extraordinarily strong deviations from scaling, as in SRIM, would result. Several previous studies have clearly shown different kinds of nonlinear behaviors, different from the scaling employed in the program, in excellent agreement with more straightforward analysis performed in transmission [30,42]. The overall uncertainty of deduced data has several components: A systematic uncertainty comes from the thickness calibration via RBS which in turn is dominated by inaccuracies of the energy loss in the Si substrate and potential channeling in the substrate, as well as counting statistics. RBS measurements were performed off axis with multiple small angular movements of the sample around an equilibrium position. Nevertheless, residual channeling was found to be difficult to suppress to a level below 3% [52]. The Si stopping is claimed to be known with accuracy significantly better than 1% [53]. Counting statistics is also expected to contribute on a level of about 2% to the uncertainties. In total, a conservative estimate yields thus 4%–5% systematic error due to the thickness calibration for the final stopping cross sections deduced. From the evaluation by TRBS, a minor statistical uncertainty due to the fitting procedure may be expected below 2% as can be estimated from Fig. 1 with simulations with $\pm 4\%$ in $\varepsilon$ compared to the best fit. Taking into account possible additional uncertainties due to film stoichiometry, binning effects, etc., the cumulative uncertainty of deduced stopping cross

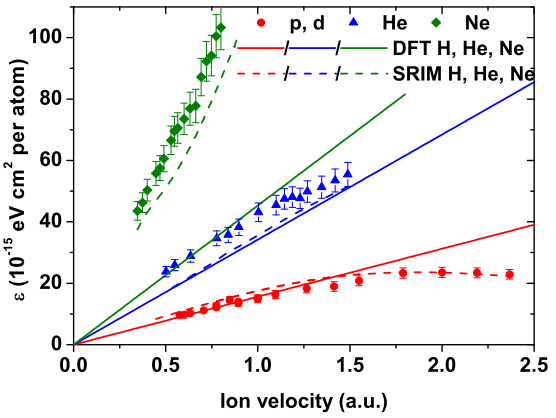


FIG. 3. Experimental electronic stopping cross sections $\varepsilon$ for H, He, and Ne ions in titanium nitride (full circles, triangles, and diamonds in red, blue, and green, respectively). Also shown are predictions by SRIM (dashed lines) and by DFT (solid lines).

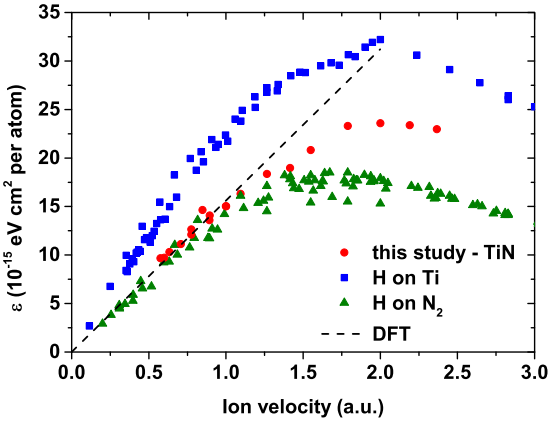


FIG. 4. Electronic stopping cross section $\varepsilon$ per atom of TiN (red circles), metallic Ti (blue squares), and $N_2$ gas (green triangles) for H ions (data for Ti and $N_2$ taken from [57]). The dashed line indicates the prediction by DFT in accordance with the electron density deduced from the plasmon frequency of TiN.

sections should not exceed 7%, with the highest uncertainties for the lowest energies. Note that the majority of the errors have a systematic character, as also the statistical error from RBS enters evaluation as a systematic uncertainty in thickness. Thus such an error would introduce mainly a scaling factor, leaving velocity and energy scaling of the obtained data unaffected.

Finally, a potential influence of the large-angle scattering event has to be discussed: For the present study, employed films lead to path lengths on the order of more than 300 Å in TiN. This situation minimizes the contribution from additional larger inelastic energy losses in the backscattering collisions. Even if such processes under certain circumstances can dissipate up to several hundred eV due to the small impact parameter the total energy losses observed are much larger (e.g., up to several tens of keV for Ne). For the same reason, a possibly enhanced stopping cross section due to increased ionic charge state after the large-angle collision is expected to have only minor impact. Typical neutralization rates for, e.g., He ions are on the order of at least $10^{15}$/s, which for 100 keV He implies neutralization within at most 1 nm [54].

## III. RESULTS AND DISCUSSION

In Fig. 3 we present the experimental results for the electronic SCS of H, He, and Ne in TiN. A comparison of our results to data from the literature is not presented here as we have not found any available data, despite the technological relevance of TiN in thin-film applications [55,56]. Nevertheless, Fig. 3 holds predictions by SRIM for the projectiles of interest (dashed lines). Considering the fact that these predictions are based on extrapolation from other materials and on Bragg's rule, the SRIM data are surprisingly precise, with deviations less than 20% with respect to our data. The error bars for all data depict the cumulative uncertainty including both statistical errors and a dominant contribution from possible systematic errors. Note that no systematic difference between data obtained from sputtered and arc-deposited thin films has been found, which indicates the absence of sample preparation bias.

For protons $\varepsilon$ is found to be proportional to velocity, as has been observed for many metals and compounds, at velocities below 1 a.u. In absolute terms it is one of the lowest SCS values observed so far for protons, corresponding to a stopping power of $\sim$10 eV/Å for 10 keV protons. At a velocity of $\sim$2 a.u., corresponding to a proton energy of $\sim$100 keV, the SCS exhibits its maximum, with a value of $\sim 22\times10^{-15}$ eV cm$^2$/atom. Note that the position of the Bragg peak points towards contribution of both conduction electrons and low-lying atomic levels to the stopping process, since in the absence of a contribution of atomic levels, the stopping power maximum is found at lower proton velocities, e.g., at 60 keV for protons in Al [57].

For He, the SCS data exhibit a linear velocity dependence, but no proportionality, since in contrast to $\varepsilon$ for protons, the extrapolation of the SCS to $v = 0$ leads to a positive threshold of $(5.6 \pm 0.7)\times10^{-15}$ eV cm$^2$/atom. Even if this value is meaningless if taken literally, it contains interesting information in the sense that it points towards an additional mechanism of energy transfer to the electronic system, apart from electron-hole pair excitation in Coulomb collisions, which seems to be the dominant mechanism of energy loss for protons (see below). For Ne, the SCS exhibits again velocity proportionality within the experimental uncertainties. In order to shed light on the observed features in electronic stopping of TiN for the projectiles of interest, we compare our results to available data for metallic Ti and $N_2$ gas (data extracted from [57]).

Figures 4 and 5 compare the present experimental data for H and He ions in TiN to experimental data for Ti and $N_2$. Note that all data are presented as electronic stopping cross sections per atom. Interestingly, for hydrogen and low energies, data for $N_2$ and TiN are found to coincide. Only for ion velocities exceeding 1 a.u., data for TiN are found to exceed the data for N ending up with the average value of the observed stopping cross sections for Ti and $N_2$ at the highest energies investigated. Thus, at the highest employed energies, i.e., when the maximum energy transfer is large enough to wash out band structure effects, Bragg's rule is found perfectly valid, while at lower energies, where excitations are limited to valence states, the electronic energy loss seems to be dominated by N. This

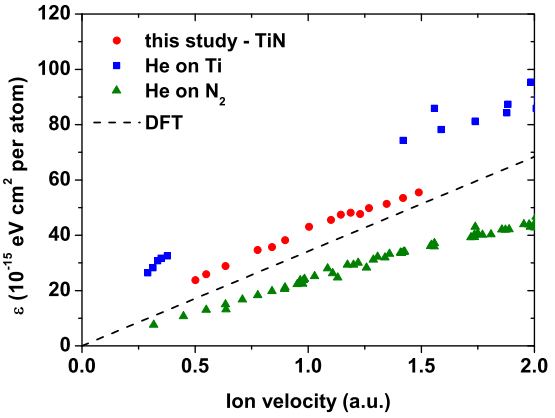


FIG. 5. Electronic stopping cross sections $\varepsilon$ per atom for TiN (red circles), metallic Ti (blue squares), and $N_2$ gas (green triangles) for He ions (data for Ti and $N_2$ taken from [57]). The dashed line indicates the prediction by DFT in accordance with the electron density deduced from the plasmon frequency of TiN.

interpretation is supported by calculations for the density of states for TiN, which indicate that the majority of electrons in the valence and conduction band are found in states associated with the nitrogen atoms [58].

For He, in contrast, experimental data show a different behavior. Here, at all investigated energies, the stopping cross sections as determined for TiN are exceeding the values for N significantly. Even if experimental data are scarce for the constituting elements, in particular for Ti, data seem to follow Bragg's rule well, although such a behavior is not expected at the present energies, as exemplified by the results for protons.

To shed light onto the energy-loss mechanisms, we also compare our results to predictions by nonlinear theory. Therefore, Figs. 3–5 also hold results from a calculation for a free-electron gas according to the nonlinear DFT model by Nagy *et al.* [22] and Echenique *et al.* [23].

For TiN, $\hbar\omega_{\mathrm{p,expt}}$ is 23 eV [59,60], corresponding to $r_s = 1.61$ and $Q_H = 0.291$ a.u. Thus, for a FEG density as deduced from the experimental plasmon energy, virtually quantitative agreement is obtained for H up to a velocity of $\sim$1 a.u. Note that a density parameter of 1.61 corresponds to 6.8 electrons per TiN molecule in very good agreement with expectation from the available electronic states at low binding energies (Ti $4s$ and $3d$ + N $2p$) which sum up to 7 electrons per molecule.

For He ions, the theoretical prediction agrees reasonably well with experimental data for velocities above 1.15 a.u. At lower velocities, the experimental data increasingly exceed the theoretical values by up to 25%, and a naïve linear extrapolation of the experimental data would lead to a SCS value of $\varepsilon \sim 5.6\times10^{-15}\,\mathrm{eV\,cm^2/atom}$ at vanishing velocity. This value is *per se* meaningless, but instead points towards an additional energy-loss mechanism setting prominent at lower velocities, contributing additionally to electron-hole pair excitation. In fact, the magnitude of the electronic energy loss below 1 a.u. could only be explained by the presence of around 11 atoms per molecule ($r_s = 1.4$), which would include significant contributions from inner shells. Interestingly, the experimental data are found to show an almost constant deviation from the DFT predictions. Note that also the data presented for Ti as a comparison show a similar behavior.

Interestingly, the data obtained for Ne ions exceed the DFT results by almost a factor of $\sim$3 when interpolating the calculations for different electron gas densities in Ref. [22]. This result clearly shows that the physical situation of electronic stopping in polycrystalline TiN is very much different from channeling conditions in a Si single crystal. The huge electronic stopping power in TiN for Ne ions can also be traced back to the contribution of a second energy-loss mechanism, in addition to Coulomb excitation, which for Ne ions is even more effective than for He, but is not possible for H ions.

The more complex behavior observed for the SCS of TiN for He and Ne ions is in line with a series of recent investigations indicating different energy-loss mechanisms active for protons and heavier ions [41,42]. For He, charge exchange cycles have been proposed as a possibility to account for the additional energy loss observed. A recent investigation of Auger emission spectra could show that indeed inner shell excitation such as Al $2p$ by He ions is possible well below 1 a.u. [44], being related to charge exchange and internal projectile excitation. Also for Ti, the impact of comparably slow but more complex ions such as Kr has been shown to be able of excitation of Ti $3p$ levels [61]. If repeated charge exchange cycles would act as a driving force for excitation different from direct electron-hole pair excitation, the observed scaling of the electronic stopping cross section for He could be understood, i.e., a constant contribution at different energies indicates a process with only weak energy dependence which is transferring repeatedly a certain quantum of energy along the ion trajectory.

## IV. SUMMARY AND CONCLUSIONS

In the present study, experimentally deduced stopping cross sections for protons, He, and Ne ions in TiN are presented. The results for protons indicate that the observed SCS is due to excitation of conduction electrons by protons via Coulomb collisions, since the data are perfectly well described by theory in accordance with the electronic structure of TiN. Also, data for Ne exhibit velocity proportionality to electronic stopping, but with a much higher SCS than predicted by theory, which points towards the efficient contribution of an additional excitation mechanism, different from direct excitation of electron-hole pairs in ion-electron interactions. Electron promotion in atomic collisions or other charge exchange processes may be a realistic candidate for this process [62]. This assumption is supported by the SCS of He, which exceeds the prediction systematically, but with less pronounced deviations. Moreover, for He ions instead of the expected velocity proportionality a linear velocity dependence is observed so that extrapolation of the data to $v = 0$ yields nonvanishing electronic stopping of ions at rest. The present data thus indicate an increasing contribution of processes different from direct collision induced electron excitation to the electronic SCS. Within the investigated energy range the additional losses exceeding DFT predictions exhibit no clear velocity or energy dependence.

Excitations of atomic levels such as Ti $3p$ combined with a sequence of excitation and decay processes within the He ion or atom system along the ion trajectory are proposed as an

explanation of the observed features in the SCS, in accordance with recent studies on electronic energy loss and Auger electron emission. A thorough theoretical description with time-dependent density functional theory accurately modeling the contribution from inner shells could shed light on the relevance of the proposed dynamical processes. At the same time, additional experimental investigations including studies of projectile charge states after interaction are expected to yield important complementary information.


## ACKNOWLEDGMENTS

The authors would like to acknowledge support of accelerator operation in Uppsala by the Swedish Foundation for Strategic Research SSF in the form of an infrastructure fellowship (RIF14-0053). Financial support by the Austrian Science Fund FWF (Project No. P25704-N20) is gratefully acknowledged. B.B. acknowledges support through a travel scholarship by the Wilhelm Macke Foundation.



[1] S. Kim, S. Lee, and J. Hong, ACS Nano **8**, 4698 (2014).
[2] X. Liu, P. K. Chu, and C. Ding, Mater. Sci. Eng., R **47**, 49 (2004).
[3] I. Monnet, C. Grygiel, M. L. Lescoat, and J. Ribis, J. Nucl. Mater. **424**, 12 (2012).
[4] S. Limandri, P. de Vera, R. C. Fadanelli, L. C. C. M. Nagamine, A. Mello, R. Garcia-Molina, M. Behar, and I. Abril, Phys. Rev. E **89**, 022703 (2014).
[5] E. Strub, W. Bohne, S. Lindner, and J. Röhrich, Surf. Interface Anal. **35**, 753 (2003).
[6] E. Guziewicz, A. Turos, A. Stonert, D. Snigurenko, B. S. Witkowski, R. Diduszko, and M. Behar, Thin Solid Films **612**, 337 (2016).
[7] P. E. Grabowski, M. P. Suhr, D. F. Richards, F. R. Graziani, and M. S. Murillo, Phys. Rev. Lett. **111**, 215002 (2013).
[8] B. Da, H. Shinotsuka, H. Yoshikawa, Z. J. Ding, and S. Tanuma, Phys. Rev. Lett. **113**, 063201 (2014).
[9] D. Belkić, J. Math. Chem. **47**, 1366 (2010).
[10] P. Sigmund, ICRU News (2000) (unpublished).
[11] E. Rutherford, Philos. Mag. Ser. 6 **21**, 669 (1911).
[12] G. Schiewitz, P. L. Grande, C. Auth, H. Winter, and A. Salin, Phys. Rev. Lett. **72**, 2159 (1994).
[13] W. Brandt and M. Kitagawa, Phys. Rev. B **25**, 5631 (1982).
[14] D. I. Thwaites, Nucl. Instrum. Methods Phys. Res., Sect. B **69**, 53 (1992).
[15] P. Bauer, R. Golser, D. Semrad, P. Maier-Komor, F. Aumayr, and A. Arnau, Nucl. Instrum. Methods Phys. Res., Sect. B **136–138**, 103 (1998).
[16] W. H. Bragg and R. Kleeman, Philos. Mag. **10**, 318 (1905).
[17] E. Fermi and E. Teller, Phys. Rev. **72**, 399 (1947).
[18] J. Lindhard, *On the Properties of a Gas of Charged Particles*, Mathematisk-Fysiske Meddelelser (Munksgaard, Copenhagen, 1954), Vol. 28, p. 1.
[19] R. H. Ritchie, Phys. Rev. **114**, 644 (1959).
[20] D. Isaacson, New York University, University Document No. 02698 (1975).
[21] P. M. Echenique, R. M. Nieminen, J. C. Ashley, and R. H. Ritchie, Phys. Rev. A **33**, 897 (1986).
[22] I. Nagy, A. Arnau, and P. M. Echenique, Phys. Rev. A **40**, 987 (1989).
[23] P. M. Echenique, F. Flores, and R. H. Ritchie, Solid State Phys. **43**, 229 (1990).
[24] F. H. Eisen, Can. J. Phys. **46**, 561 (1968).
[25] M. Peñalba, A. Arnau, and P. M. Echenique, Nucl. Instrum. Methods Phys. Res., Sect. B **67**, 66 (1992).
[26] J. E. Valdés, Nucl. Instrum. Methods Phys. Res., Sect. B **73**, 313 (1993).
[27] A. Mann and W. Brandt, Phys. Rev. B **24**, 4999 (1981).
[28] J. E. Valdés, J. C. Eckardt, G. H. Lantschner, and N. R. Arista, Phys. Rev. A **49**, 1083 (1994).
[29] E. A. Figueroa, E. D. Cantero, J. C. Eckardt, G. H. Lantschner, J. E. Valdés, and N. R. Arista, Phys. Rev. A **75**, 010901 (2007).
[30] S. N. Markin, D. Primetzhofer, M. Spitz, and P. Bauer, Phys. Rev. B **80**, 205105 (2009).
[31] M. A. Zeb, J. Kohanoff, D. Sánchez-Portal. A. Arnau, J. I. Juaristi, and E. Artacho, Phys. Rev. Lett. **108**, 225504 (2012).
[32] E. E. Quashie, B. C. Saha, and A. A. Correa, Phys. Rev. B **94**, 155403 (2016).
[33] C.Auth, A. Mertens, H. Winter, and A. Borisov, Phys. Rev. Lett. **81**, 4831 (1998).
[34] R. Golser and D. Semrad, Phys. Rev. Lett. **66**, 1831 (1991).
[35] S. N. Markin, D. Primetzhofer, and P. Bauer, Phys. Rev. Lett. **103**, 113201 (2009).
[36] B. Solleder, L. Wirtz, and J. Burgdörfer, Phys. Rev. B. **79**, 125107 (2009).
[37] J. M. Pruneda, D. Sánchez-Portal, A. Arnau, J. I. Juaristi, and E. Artacho, Phys. Rev. Lett. **99**, 235501 (2007).
[38] A. Lim, W. M. C. Foulkes, A. P. Horsfield, D. R. Mason, A. Schleife, E. W. Draeger, and A. A. Correa, Phys. Rev. Lett. **116**, 043201 (2016).
[39] G. Schiwietz and P. L. Grande, Nucl. Instrum. Methods Phys. Res., Sect. B **175–177**, 125 (2001).
[40] M. Behar, R. C. Fadanelli, I. Abril, R. Garcia-Molina, C. D. Denton, L. C. C. M. Nagamine, and N. R. Arista, Phys. Rev. A **80**, 062901 (2009).
[41] D. Primetzhofer, Phys. Rev. A **89**, 032711 (2014).
[42] D. Primetzhofer, S. Rund, D. Roth, D. Goebl, and P. Bauer, Phys. Rev. Lett. **107**, 163201 (2011).
[43] P. Riccardi, A. Sindona, and C. A. Dukes, Nucl. Instrum. Methods Phys. Res., Sect. B **382**, 7 (2016).
[44] P. Riccardi, A. Sindona, and C. A. Dukes, Phys. Lett. A **381**, 1174 (2017).
[45] G. Greczynski, S. Mráz, L. Hultman, and J. M. Schneider, Appl. Phys. Lett. **108**, 041603 (2016).
[46] Y. Zhang, H. J. Whitlow, T. Winzell, I. F. Bubb, T. Sajavaara, K. Arstila, and J. Keinonen, Nucl. Instrum. Methods Phys. Res., Sect. B **149**, 477 (1999).
[47] M. A. Arvizu, R. Wen, D. Primetzhofer, J. E. Klemberg-Sapieha, L. Martinu, G. A. Niklasson, and C. G. Granqvist, ACS Appl. Mater. Interfaces **7**, 26387 (2015).
[48] M. K. Linnarsson, A. Hallén, J. Åström, D. Primetzhofer, S. Legendre, and G. Possnert, Rev. Sci. Instrum. **83**, 095107 (2012).
[49] N. Klingner, R. Heller, G. Hlawacek, J. von Borany, J. Notte, J. Huang, and S. Facsko, Ultramicroscopy **162**, 91 (2016).

[50] J. P. Biersack, E. Steinbauer, and P. Bauer, Nucl. Instrum. Methods Phys. Res., Sect. B **61**, 77 (1991).
[51] J. F. Ziegler, M. D. Ziegler, and J. P. Biersack, Nucl. Instrum. Methods Phys. Res., Sect. B **268**, 1818 (2010).
[52] A. L'Hoir, D. Schmaus, J. Cawley, and O. Jaoul, Nucl. Instrum. Methods Phys. Res. **191**, 357 (1981).
[53] N. P. Barradas, E. Alves, Z. Siketić, and I. B. Radović, in *Application of Accelerators in Research and Industry—2008, Fort Worth, TX*, edited by F. D. McDaniel and B. L. Doyle, Proceedings of the Twentieth International Conference, AIP Conf. Proc. No. 1099 (AIP, New York, 2009).
[54] D. Primetzhofer, S. N. Markin, J. I. Juaristi, E. Taglauer, and P. Bauer, Nucl. Instrum. Methods Phys. Res., Sect. B **267**, 624 (2009).
[55] M. Wittmer and H. Melchior, Thin Solid Films **93**, 397 (1982).
[56] S. Piscanec, L. C. Ciacchi, E. Vesselli, G. Comelli, O. Sbaizero, S. Meriani, and A. de Vita, Acta Mater. **52**, 1237 (2004).
[57] Available from https://www-nds.iaea.org/stopping/.
[58] C. Ortiz, O. Eriksson, and M. Klintenberg, Comput. Mater. Sci. **44**, 1042 (2009).
[59] P. Prieto and R. E. Kirby, J. Vac. Sci. Technol., A **13**, 2819 (1995).
[60] C. G. H. Walker, C. A. Anderson, A. McKinley, N. M. D. Brown, and A. M. Joyce, Surf. Sci. **383**, 248 (1997).
[61] T. E. Gallon, K. Orgassa, and J. A. D. Matthew, J. Phys.: Condens. Matter **7**, 8539 (1995).
[62] U. Wille and R. Hippler, Phys. Rep. **132**, 129 (1986).